J. Phys. Chem. A **2008,** *112,* 4965–4972

Direct Metal−Metal Interaction Contributions to Quadratic Hyperpolarizability: A Study on Dirhenium Complexes

Qiaohong Li, Rongjian Sa, Yongqin Wei, and Kechen Wu*

State Key Laboratory of Structural Chemistry, Fujian Institute of Research on the Structure of Matter, Chinese Academy of Sciences, Fuzhou 350002, People's Republic of China

Received: December 29, 2007; Revised Manuscript Received: March 11, 2008

We present a comparative study of the metal−metal interaction effect on the static quadratic hyperpolarizabilities of two typical dinuclear rhenium clusters. The electronic structures, excitation spectra, dipolar moments, static polarizabilities, and quadratic hyperpolarizabilities of the two complexes with direct metal−metal interactions have been computed and analyzed with the use of high-level DFT/TDDFT methods. The geometries and the first intense excitations agree with the relevant reported measurements. The orbital decomposition scheme (*J. Phys. Chem. A* **2006**, *110*, 1014−1021) has been applied to analyze the relationship between the electronic structures and nonlinear optical (NLO) properties of these two complexes. We propose an unprecedented NLO response mechanism featuring the contribution of the direct metal−metal interaction transition process in these dinuclear rhenium complexes. This contribution positively enhances the quadratic hyperpolarizability and relates to the intensity of the metal−metal interactions of the complexes. The results are helpful to the development of NLO chromophores in polynuclear metal clusters through the molecular design technique.

1. Introduction

In the past two decades, the organometallic nonlinear optical (NLO) chromophores have attracted great interest.[1–3] Introducing the heavy metal atoms into the pure organic molecules brings vast opportunities to the enhancement of the quadratic hyperpolarizability (β) due basically to the reinforcement of push−pull charge transfer (CT) of NLO chromophores. Since the pioneering work of Frasier[4] and Green[5] on the ferrocene derivative complexes, the record-holder of the "highest" title of the static quadratic hyperpolarizability of transition-metal-based NLO-phores keeps changing and is now a metalloporphyrin chromophore [the push−pull arylethyny(porphinato)zinc derivative] possessing the *static* quadratic hyperpolarizability value up to 800×10^{-30} esu (dynamic value at 1064 nm is up to 5000×10^{-30} esu).[6] The metal-based chromophores with sufficiently large second-order NLO activities have potential applications in the telecommunication area, data storage, computer, and display technologies.

Many desirable material properties tend to have tradeoffs; for example, the known nonlinearity-transparency tradeoff in developing the novel NLO crystals.[7] The enhanced quadratic hyperpolarizabilities of organic or organometallic molecules are sometimes accompanied by the red-shift in their optical absorption into the visible part or even into the near-to-mid-IR part of the spectrum, limiting their practical *nonresonance applications* in this frequency range. The large quadratic hyperpolarizability of a push−pull organometallic NLO-phore to a high degree rests in the extension of π-conjugated ligands (such as the longer π-conjugated backbone of ligands in tetrahedral or octahedral octupolar organometallic NLO-phores[8]), which play the key role in the metal-to-ligand CT (MLCT) or/and metal inductive ligand-to-ligand (LLCT)/intraligand CT (ILCT). However, the more extended conjugated ligand (such as a very long π-conjugated backbone) may bring on the unfavorable red-shift absorptions and/or in some cases the crystallization difficulties, which seriously restricts the *resonant* applications as solid-state organometallic NLO crystals. Moreover, some studies have revealed that the β values of some dipolar NLO-phores cannot be further enhanced by lengthening the conjugated π backbone.[9] The more favorable pathway in developing the transition-metal-containing NLO-phores is expected to improve the tradeoffs between the nonlinearity and the transparency and/or the crystallizability.

The metal−metal interactions arouse great interest in both fundamental chemistry and potential material research.[10] Since Cotton's report on the first quadruple Re−Re bonding,[11] great efforts have been made to maximize the bond order between two transition-metal atoms, and most recently, great achievements have made on dinuclear chromium complexes.[12,13] In addition to the multiple direct metal−metal bonding being essentially interesting from a fundamental point of view, most reported synthetic organometallic complexes with *indirect* metal−metal interactions show some promising physical and chemical properties.[14] The general picture of hetero- and homogeneous bimetallic complexes stabilized by an unsaturated bridging ligand can produce bright luminescent light in the visible spectroscopic region characterized by the metal-to-ligand-to-metal charge transfer (MLM'CT) excitation modified by metal−metal interactions.[15] Some studies have also ascribed the second-order NLO properties to the *indirect* metal−metal interactions of some mixed-valence bimetallic ruthenium complexes, [16] dinuclear metallocene derivatives,[17] and metal sesquifulvalence complexes.[18] Consequently, it follows a rational line to come to the study on the *direct* metal−metal interaction, strong multiple bonding or weak coupling, relating to the NLO activities of polynuclear metal cluster compounds.

Although the NLO properties of the polynuclear transition-metal cluster compounds have been studied for about two decades, the reports until now have been limited to the

---

* To whom correspondence should be addressed. E-mail: wkc@fjirsm.ac.cn.

10.1021/jp712156t CCC: $40.75

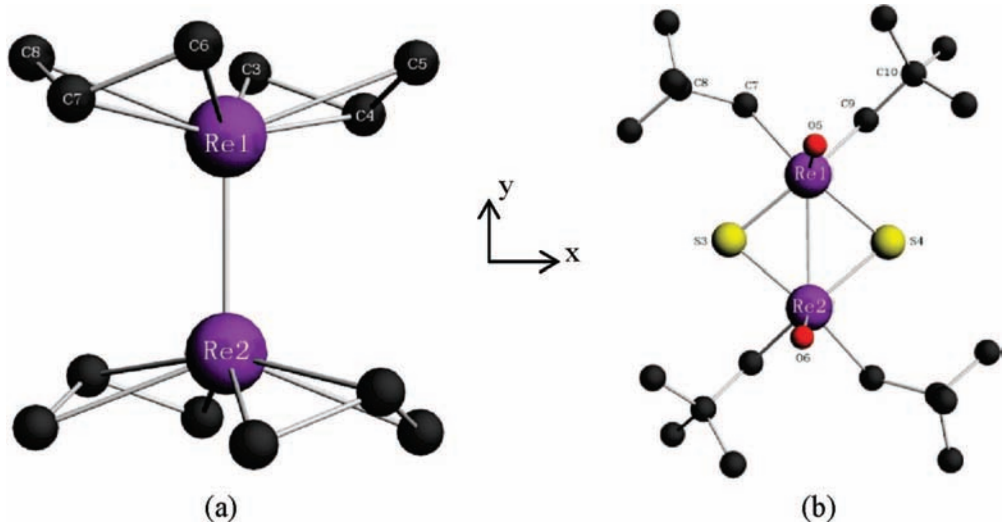

Figure 1. Molecular structures of the model complexes (a) $Re_2(allyl)_4$; (b) $Re_2(\mu\text{-}S)_2O_2(CH_2CMe_3)_4$. H atoms are omitted for clarity.

measurements of third-order NLO activities such as the optical limiting properties.[19–21] They have provided invaluable information in which the transition-metal nature is discussed in some ways. Alternatively, to the best of our knowledge there are only a few reports on the potential *second-order* NLO activities of the polynuclear cluster compounds,[22,23] saying nothing of the potential applications such as in the optical telecommunication area as switches and modulators. Moreover, the second-order NLO nature of the polynuclear metal clusters remains unclear in contrast to that of the organometallic or metal-free organic NLO-phores. The *direct* metal−metal interactions that uniquely exhibit in the polynuclear clusters are expected to play certain roles in the NLO response mechanism.[22] This motivates us to investigate the structure−NLO property relationship of polynuclear metal clusters, which may lead to a new way to develop favorable metal-based NLO-phores with increased optical transparency and crystallizability while maintaining relatively large NLO responses.

The experimental report on molecular quadratic hyperpolarizabilities is very limited of the polynuclear cluster compounds. This would bring difficulty in the theoretical analysis, but some *indirect* experimental results of the photophysical properties of the polynuclear clusters are very informative to consult with.[24] On the basis of the above consideration, in this paper two typical dinuclear rhenium cluster complexes have been chosen as the theoretical models. One is the $[Re(C_3H_5)_2]_2$ complex (**1**) (we note the organic ligand C_3H_5 as allyl in the following), which contains a very strong direct metal−metal interaction[25] (Re−Re triple bond reported by Cotton et al.[26]), and the other one is $[Re(\mu\text{-}S)OL_2]_2$ $[L{=}(CH_2CMe_3)]$ complex (**2**) containing a relatively weak direct metal−metal interaction.[27] These two models are selected carefully in terms of enough simple structures and acentric space group symmetry of the corresponding single crystals, which is necessary for producing macroscopic second-order NLO activities (both are in monoclinic C_2 symmetry). These two models are dimerized by two equivalent moieties, that is, the $Re(C_3H_5)_2$ moiety for **1** and the $Re(\mu\text{-}S)OL_2$ moiety for **2**. The notably different metal−metal interactions in these two models provide a useful comparative example to analyze their contributions to the quadratic NLO response.

The recently proposed orbital decomposition scheme by Hieringer and Baerends[28] provides a very useful tool to relate the electronic structures and the relevant orbital-pair transitions to the quadratic hyperpolarizability. It is based on the response theory and has been confirmed useful by the previous study in understanding the quadratic NLO nature of organometallic chromophores.[29] Another advantage of the decomposition scheme lies in the economic computational burden. It could be obtained as a byproduct of the quadratic hyperpolarizability calculations without any additional computations. So it is particularly useful to the complex sizable systems like the polynuclear metal-based NLO-phores. The present study on the dirhenium complexes mostly builds upon the orbital decomposition analysis.

The paper is organized as follows. In Section 2, we first describe the density functional (DFT) and time-dependent DFT computational methods as well as the modified orbital decomposition scheme used in the present study. In Section 3, two typical bimetallic rhenium complexes are studied and analyzed on the geometries, electronic structures, excitation spectra, and static quadratic hyperpolarizability. The structure−NLO property relationships are discussed with the focus on the metal−metal interactions and their comparable contributions to the quadratic hyperpolarizability. In Section 4, we draw some conclusions based on the calculations and NLO response mechanism analyses.

2. Computational Methods

The initial geometric structures of the two dirhenium models were taken from the X-ray diffraction data.[26,27] The molecular geometries illustrated in Figure 1 were fully optimized with C_2 symmetric restriction to the local energy minima, which have been confirmed by no imaginary harmonic vibration frequency. The twofold axes of both models were arranged to be along Cartesian *z* axes, which are also identical to their dipole moment directions. The selected experimental and computed geometric parameters such as the bond lengths and angles are listed in Table 1.

The geometric optimizations and ground-state self-consistent-field (SCF) calculations were proceeded at the triple-ζ split-valence Slater orbital-type basis set with two augumented polarization functions (TZ2P) and the “small” frozen core level: (Re:4d; O:2s; S:2s; N:2s). The Becke−Perdew (BP) pure general gradient approximation (GGA) exchange-correlation (XC) functional[30] was used with the local density approximation (LDA) part being VWN type[31] including the Stoll correction.[32] The

TABLE 1: Selected Experimental (in Parentheses) and Calculated Bond Lengths (Å) and Angles (deg) of Models 1 and 2

1		2	
Re1−Re2	2.277 (2.217)	Re1−Re2	2.843 (2.759)
Re1−C3	2.194 (2.150)	Re1−S3	2.293 (2.237)
Re1−C4	2.200 (2.180)	Re1−S4	2.344 (2.242)
Re1−C5	2.196 (2.239)	Re1−O5	1.695 (1.729)
Re1−C6	2.196 (2.182)	Re1−C7	2.218 (2.142)
Re1−C7	2.200 (2.146)	Re1−C12	2.234 (2.165)
Re1−C8	2.196 (2.205)	C7−C8	1.560 (1.652)
C3−C4	1.438 (1.384)	C9−C10	1.562 (1.539)
C3−C5	1.438 (1.409)		
C4−C5	2.470 (2.481)	S3−Re1−S4	97.4 (99.2)
C6−C7	1.438 (1.387)	S3−Re1−O5	118.8 (114.6)
C6−C8	1.438 (1.469)	S3−Re1−C7	83.0 (85.7)
C7−C8	2.470 (2.492)	S3−Re1−C9	132.7 (135.0)
		S4−Re1−O5	110.7 (109.1)
C3−Re1−C4	38.2 (37.2)	S4−Re1−C7	145.9 (145.4)
C3−Re1−C5	68.5 (68.8)	S4−Re1−C9	77.5 (77.9)
C4−Re1−C5	38.2 (37.2)	O5−Re1−Re2	107.7 (106.8)
C6−Re1−C7	38.2 (37.4)	O5−Re1−C7	98.4 (99.5)
C6−Re1−C8	68.4 (69.2)	O5−Re1−C9	108.4 (108.4)
C7−Re1−C8	38.2 (39.4)		

fitted electron density was used in the calculation of the XC potential. The scaled-ZORA Hamiltonian[33] was used to take account of the relativistic effect in the calculations. The SCF procedures were converged to 10^{-8} au, and the integration accuracy parameter was set to 5. The computational scheme described above would be adopted for all of the following calculations except the alteration of the GGA part of the XC functional for the response property calculations. All of the calculations were performed with the Amsterdam density functional program (ADF 2006.01 version)[34] on a DELL Poweredge server.

The electronic excitation properties and the quadratic hyperpolarizabilities of models **1** and **2** were calculated by using the response theory implemented in the RESPONSE module[35] of the ADF program. The GGA part of the XC functional in these cases employed the gradient-regulated asymptotic connection (GRAC)[36] of the potentials based on the BP functional and the shape-corrected LB94 potential proposed by van Leeuwen and Baerends[37] designed particularly for response properties. The Davidson diagonalization method was used to yield the excitation information. Totally, 200 excited states with nonzero oscillator stengths were calculated for the two models. The molecular symmetry (C_2) was turned off during the analytical TDDFT calculations for the polarizabilities and quadratic hyperpolarizabilities. Only the static values of two model clusters have been calculated because of the absence of the comparative experimental dynamic data. Recently, there have been many valuable reports on the TDDFT calculations of the hyperpolarizability for the transition-metal-containing chromophores.[9a,28,29,38] The orientationally averaged static values of the polarizability (α) and quadratic hyperpolazribility (β) are defined as follows:

$$\bar{\alpha} = \frac{1}{3}(\alpha_{xx} + \alpha_{yy} + \alpha_{zz}) \tag{1}$$

$$\bar{\beta} = \sqrt{\sum_i \beta_i^2} \tag{2}$$

$$\beta_i = \frac{3}{5} \sum_{j=x,y,z} \beta_{ijj} \quad i = x, y, z \tag{3}$$

The orbital-decomposition scheme proposed by Hieringer and Baerends was adopted to analyze the contribution of the relevent orbital-pair transitions to the β. The theoretical base of the decomposition scheme has been described in detail elsewhere.[28] The formulation of the β induced by the orbital-pair transition was described as follows:[29]

$$\beta_{(a,b)}^{\mathrm{CT}} = \sum_i^N \frac{\Delta u_i c_{(a,b)} M_{(a,b)}^2}{\Delta E_i^2} \tag{4}$$

where (a, b) is an orbital-pair transition involved in the ith electronic excitation; $M_{(a,b)}$ is the transition dipole moment in the ith excitation; $C_{(a,b)}$ is the weight factor of the (a, b) transition in the ith excitation; ΔE_i is the transition energy of the ith excitation. The summation is over all of the excitations that possess the (a, b) orbital-pair transition ($N = 200$ in our case). $\Delta\mu_i$ is the difference of the transition dipole moment between the ith excited state and the ground state. It is obtained by using the finite-field method with the finite field of 0.001 au.[39] By using this scheme, the relative contribution to β_{CT} of a specified orbital-pair transition with respect to that of another orbital-pair transition can be shown clearly. The calculated static $\beta_{(a,\ b)}$ of both models with the dominant percentages and relative ratios were listed in Table 3.

TABLE 2: Selected Bond Orders of Models 1 and 2 Obtained by the Mayer Method

1		2	
Re1−Re2	2.00	Re1−Re2	0.65
Re1−C3	0.33	Re1−S3	1.01
Re1−C4	0.58	Re1−S4	0.93
Re1−C5	0.33	Re1−O5	1.79
Re1−C6	0.33	Re1−C7	0.74
Re1−C7	0.58	Re1−C9	0.77
Re1−C8	0.33		

Because of the lack of measured data available for the β of the two dirhenium complexes, the present computed values were largely qualitatively valuable. On the basis of this consideration, the solvent effects, intermolecular interactions, and frequency-dependent effects, which have been proven to be quantitatively important, are not included in the present qualitative evaluations of the quadratic hyperpolarizability.

3. Results and Discussions

3.1. Geometric and Electronic Structures and Re−Re Bond Properties. The $Re_2(allyl)_4$ molecule has no bridging allyl groups. The mean Re−Re bond distance is 2.225 (7) Å, which was considered effectively triple by Cotton et al.[26] The Re centers in the $Re_2(\mu\text{-}S)_2O_2L_4$ molecule have square-pyramidal geometries with the oxo ligand in the apical position and the basal plane defined by two carbons and bridging sulfide group. The Re−Re distance of 2.759 (3) Å is slightly longer than the sum of two Re atomic radii (2.741 Å), which was considered as single bond by Hoffman et al.[27] The optimized geometric parameters of both models given in Table 1 are in reasonable agreement with the experimental data. The small difference from the crystal structures can be explained by the presence of the intercluster interactions in the solid state.

The molecular structures of both models relax in general after the geometric optimizations. The Re−Re bond lengths of models **1** and **2** stretched for 0.045 Å and 0.084 Å, respectively. The various Re−C bond lengths in model **1** (e.g., $Re_1{-}C_{3-8}$ bond lengths) tend to be homogeneous after the optimization, but the average dimensions of the Re−C distances are in accord with the measurement. In model **2**, the Re−S distances elongate for 0.080 and 0.100 Å for S_3 and S_4, respectively. The Re−O distances reduce slightly for about 0.030 Å in contrast to the

TABLE 3: Orbital Decompositions of the Dominate Component β_{zzz} of Models 1 and 2 (au); Supports That the Largest Orbital-Pair Contribution Has a Relative Ratio of 100

(a, b)	β_{zzz}	ratio	dominate excitation contribution
			1
(31b, 34b)	3.4	100	17A(11%) + 22A(59%) + 25A(4%) + 27A(3%) + 30A(5%) + 39A(3%)
(30a, 34a)	2.9	88	32A(68%) + 37A(4%) + 39A(9%)
(30b, 32b)	1.7	51	2A(51%) + 3A(22%)
(31b, 33b)	0.8	23	4A(45%) + 5A(51%)
(32a, 35a)	−1.0	−28	10A(84%) + 13A(5%)
			2
(51b, 52b)	74	100	1A(99%)
(51a, 54a)	41	56	7A(3%) + 8A(35%) + 9A(44%) + 11A(9%)
(50a, 54a)	13	18	11A(3%) + 12A(3%) + 14A(40%) + 15A(46%)
(49b, 53b)	−55	−74	11A(3%) + 15A(8%) + 16A(17%) + 17A(9%) + 18A(57%)
(49b, 54b)	−13	−18	18A(6%) + 25A(8%) + 27A(5%) + 28A(10%) + 30A(7%) + 32A(21%) + 36A(15%) + 37A(4%)

enlarged averaged Re−C distance of about 0.070 Å. The optimization relaxations are within the reasonable range, but it is worth noting that the Re−Re bonding interaction reduced after the gas-phase optimization. In other words, the Re−Re interactions of the two model complexes are stronger in the solid state than those presented in the gas-phase calculations.

The Mayer bond-order method[40] was adopted to analyze the bond properties of the models. The results show the strong Re−Re bonding in model **1** and the weak Re−Re interaction in model **2**, which agree with the experiments. Table 2 listed the selected bond orders of models **1** and **2** calculated at the BP/TZ2P/S-ZORA level of DFT theory. The bond order of Re−Re of model **1** is 2.20. The relaxed structure after the gas-phase optimization sustains the strong Re−Re bonding in model **1**. On the contrary, the calculated Re−Re bond order is 0.65, indicating the much weaker interaction between two rhenium atoms in model **2**. The Re−O bond order is 1.8, indicating the double-bond nature, whereas the Re−S bond order was 1.0, showing the single bond between them. We did not adopt the natural bond orbital-based analysis (NBO) to avoid the additional computations because the bond-order number is not the focus of the present study.

The selected frontier molecular orbitals (MOs, from the HOMO-3 to the LUMO+3) are contoured in Figure 2 with the molecular orbital energies. The six frontier MOs of model **1** are composed of mostly the 5d orbitals of dirhenium. For example, the HOMO locates mainly on two Re atoms with typical δ metal−metal antibonding orbital character (noted as d_{δ^*}) in agreement with the semiempirical result of Cotton et al.[26] (Figure 1S gives another HOMO contour view of the Re−Re δ antibonding, found in the Supporting Information). The HOMO of model **2**, however, locates on both the dirhenium atoms and the sulfide ligands. The LUMO of model **2** has d_{σ^*} character as well as p_{σ^*} antibonding of the oxo ligand.

3.2. Electronic Excitations. The gas-phase excitation spectra of the two models are depicted in Figure 3 at the GRACLB/TZ2P/S-ZORA level of the TDDFT computations. The intense lowest-energy excitation peak (λ_{max}) of model **1** locates at 461 nm ($f = 0.01$). It consists of mainly the orbital-pair transition (32a, 33a) (99%), which involves the HOMO (32a) and the LUMO+2 (33a). According to the MO results shown in Figure 2, the HOMO with a symmetry locates on the two equivalent Re atoms with the δ^* character mentioned above and the LUMO+2 also locates mainly at the two Re atoms but with the metal−metal π antibonding orbital character (noted as d_{π^*}). Consequently, the λ_{max} of model **1** at 461 nm involves the $d_{\delta^*} \rightarrow d_{\pi^*}$ transition. The λ_{max} of model **2** locates at 546 nm, which red-shifts 85 nm to that of model **1**. It has a slightly weak intensity of the calculated $f = 0.008$ and is composed of mainly the orbital-pair transition of (51b, 53a) involving the HOMO (51b) to the LUMO+1 (53a). The HOMO is characterized by the p orbitals of the S atoms and the carbon atoms of L fragments (noted as L_σ) and metal−metal δ bonding (noted as

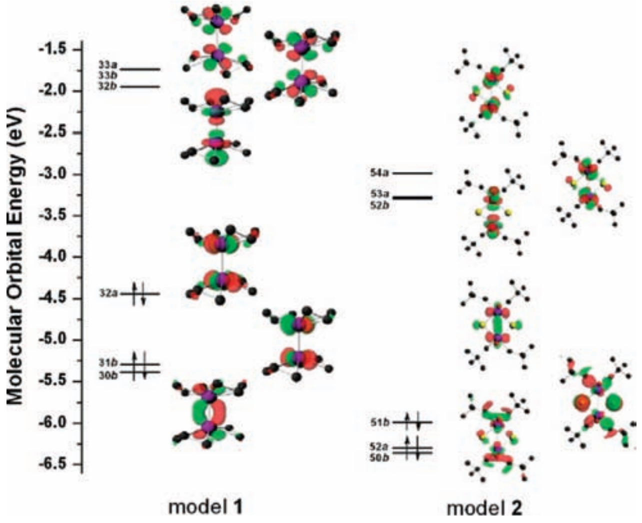

Figure 2. Frontier molecular orbital diagrams of models **1** and **2** in the DFT (BP/TZ2P/S-ZORA) calculations.

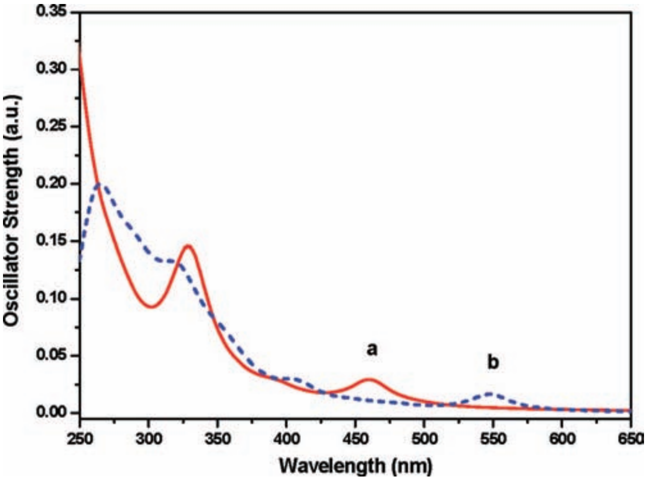

Figure 3. Simulated electronic excitation spectra of (a) model **1** (red line) and (b) model **2** (blue dash).

d_δ) of dirhenium. The LUMO+1 consists of mostly the 5d orbital components of two Re atoms with $d_{\sigma*}$ character and a small percent of p_σ antibonding orbital components of the oxo ligand ($L_{\sigma*}$). Consequently, The CT processes involved in the 1B transition are from ($L_\sigma + d_\delta$) to ($d_{\sigma*} + L_{\sigma*}$). The d → d transitions appear in both cases, but they are obviously different in intensity.

The measurements of the UV−vis spectra of these two cluster compounds at present are not available. Eglin and his collaborators have reported the intense lowest-energy absorption of another strong Re−Re coupled cluster, $[Re_2Cl(NCN)_4][BF_4]$ (the Re−Re distance is 2.224 Å, which is very closed to that of model **1**, 2.225 Å), located at 460 nm with typical d → d transition character.[24b] Some other available reports also give rise to a λ_{max} at around 420−470 nm of some dirhenium complexes containing strong Re−Re interactions.[24] In terms of these experimental reports, the TDDFT results of $\lambda_{max}(\mathbf{1})$ are reasonably accurate.

3.3. Dipole Moments, Polarizabilities, and Quadratic Hyperpolarizabilities. The TDDFT results of the ground-state dipole moments (μ), static polarizability (α), and the static quadratic hyperpolarizability (β) are distinctly anisotropic because of the specified molecular Cartesian coordinates. The μ vectors of model **1** exhibit $\mu_x = \mu_y = 0$ and $\mu_z = 0.1$ D and model **2** has $\mu_x = \mu_y = 0$ and $\mu_z = 1.8$ D. The μ_z of both models are small and have the order of $\mu_z(\mathbf{1}) \ll \mu_z(\mathbf{2})$. The calculated polarizability matrices of the two models are almost diagonal; that is, $\alpha_{ij} = 0$ ($i \neq j$). The spatially averaged $\bar{\alpha}$ value of model **1** computed from eq 1 is 33 × 10^{-24} esu, which is about one-half of that of model **2** (67 × 10^{-24} esu).

The anisotropy of the calculated static β_i values of the two models is obvious ($\beta_z \gg \beta_x, \beta_y$). The quadratic hyperpolarizability of model **1** [$\beta_z(\mathbf{1}) \approx \bar{\beta}(\mathbf{1}) = 0.6 \times 10^{-31}$ esu] is about 1 order of magnitude smaller than that of model **2** [$\beta_z(\mathbf{2}) \approx \bar{\beta}\,(\mathbf{2}) = 7.0 \times 10^{-31}$ esu]. The result is a surprise in that the second-order NLO response of model **1** with a strong Re−Re interaction is much smaller than that of model **2**, which contains a weak Re−Re interaction. The surprising result is caused by the symmetric restriction of the dimeric molecular structures, which will be explained further in Section 4.

The orbital decomposition analysis scheme has been executed on both models. The contributions of the particular occupied-virtual orbital-pair transitions (a, b) to a given quadratic hyperpolarizability (β_{zzz}, which is significant in all β_{zjj} components in eq 3 and has the relation of $\bar{\beta} \approx \beta_z \approx {}^3/_5\beta_{zzz}$) are unveiled as well as the corresponding CT processes involved in the transitions. The results are listed in Table 3 in which all other occupied to virtual orbital transitions that are computed to have lower contribution to β_{zzz} less than 5% are not listed. The lower excitation contributions less than 2% are not listed in the fourth column of the table.

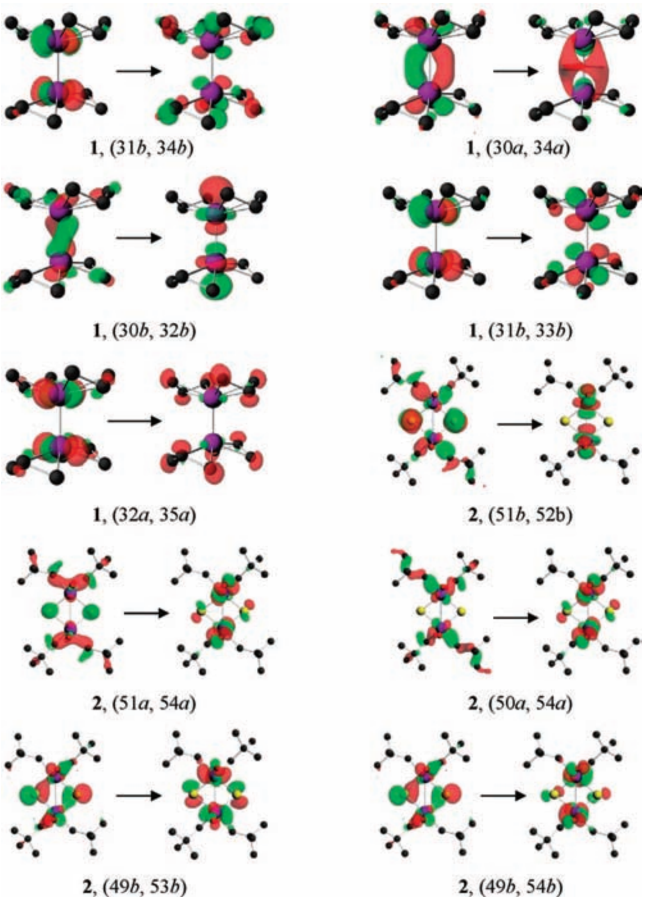
1, (31*b*, 34*b*)
1, (30*a*, 34*a*)
1, (30*b*, 32*b*)
1, (31*b*, 33*b*)
1, (32*a*, 35*a*)
2, (51*b*, 52b)
2, (51*a*, 54*a*)
2, (50*a*, 54*a*)
2, (49*b*, 53*b*)
2, (49*b*, 54*b*)

Figure 4. Illustrations of the orbital-pair transitions relevant to the quadratic hyperpolarizability of models **1** and **2** in the TDDFT (GRACLB/TZ2P/S-ZORA) calculations.

The relevant orbital-pair transitions of model **1** are multicomponent. The contributions of the first four orbital-pair transitions, that is, (31*b*, 34*b*), (30*a*, 34*a*), (30*b*, 32*b*), and (31*b*, 33*b*), have positive signs whereas the last one (32*a*, 35*a*) has a negative sign. They are all obviously characterized by predominant metal-to-metal transitions (we signify this electronic transition MMCT in this paper) as illustrated in Figure 4. The orbital pair (31*b*, 34*b*) has the largest positive contribution (the relative ratio is 100%) where 31*b* is the HOMO−1 and 34*b* is the LUMO+6. It is involved in the relatively high-energy excitations (in the range from 4.9 to 6.1 eV). We note that it is excluded in the optically intense excitation (λ_{max}). The result conflicts with the assumption of the traditional two-level model, which assumes that only the lower-energy transitions are counted. The occupied HOMO−1 is the δ bond orbital of dirhenium (d_δ), whereas the virtual LUMO+6 is dominant by the π antibond orbital of dirhenium ($d_{\pi*}$) with the fractional components of $p_{\sigma*}$ orbitals of the allyl ligands ($L_{\sigma*}$) as shown in Figure 2. This orbital-pair transition therefore involves the MMCT ($d_\delta \rightarrow d_{\pi*}$) and MLCT ($d_\delta \rightarrow L_{\sigma*}$) processes. The former process is obviously predominant (~80%). The analyses showed that the following two orbital-pair transitions of (30*a*, 34*a*) and (30*b*, 32*b*) have the second and third largest contribution to the β_{zzz} with relative ratios of 88% and 51%, respectively. Both mainly involve MMCT with $d_\pi \rightarrow d_{sd*}$ and $d_\pi \rightarrow d_{\sigma*}$ characters, respectively (d_{sd*} denotes the sd hybrid antibonding orbital of dirhenium[41]). Another orbital pair (31*b*, 33*b*) with a positive relative ratio (23%) is similar to (31*b*, 34*b*). It involves predominately MMCT ($d_\delta \rightarrow d_{\pi*}$) and fractional MLCT ($d_\delta \rightarrow L_{\sigma*}$) characters. It is worth noting that a negative contributor exists, the orbital-pair (32*a*, 35*a*). It has a non-neglectable relative ratio of about 28% to the largest one in magnitude. 32*a* is the HOMO, while 35*a* is the LUMO+4. The HOMO locates on the dirhenium with a typical δ antibond character as mentioned above, whereas the LUMO+4 locates mostly on the allyl ligands. This orbital-pair transition therefore involves mainly MLCT ($d_{\delta*} \rightarrow L_{sp*}$), where L_{sp*} denotes the sp hybrid antibonding orbitals of allyl ligands.

In a word, the metal-to-metal transition processes predominate over thē β ($\sim{}^3/_5\beta_{zzz}$) of model **1**, whereas the MLCT process could be unfavorable to the enhancement of the quadratic hyperpolarizability.

The decomposition scheme performed on model **2** shows that there are three orbital-pair transitions contributing to β_{zzz} with positive signs and there are two with negative signs. (51*b*, 52*b*) has the largest contribution, where 51*b* is the HOMO and 52*b* is the LUMO. It is involved solely in the first dark excitation (1*A*) and is again excluded from the λ_{max}-related excitation. As depicted in Figure 2, the HOMO of model **2** is no longer dominated by the 5d orbitals of dirhenium; instead, it has large components of the p orbitals of S atoms and L ligand fragments [L=(CH$_2$CMe$_3$)]: HOMO(**2**) $\approx$ 0.48p(S) + 0.27p(L) + 0.12d(Re). The LUMO, in contrast to the HOMO, is dominated by the $d_{\sigma*}$ orbitals of dirhenium with the non-negligible fractional contribution from the ligands, which is characterized mostly by the atomic p antibonding orbitals of O atoms: LUMO(**2**) $\approx$ 0.78d(Re) + 0.20p(O). Consequently, the orbital pair (51*b*, 52*b*) is revealed to be a HOMO → LUMO transition with $(L_\sigma + d_\delta) \rightarrow (d_{\sigma*} + L_{\sigma*})$ character. The relevant transition processes are multiple; that is, the dominant LMCT ($L_\sigma \rightarrow d_{\sigma*}$) and the fractional MMCT ($d_\delta \rightarrow d_{\sigma*}$) and metal-inductive LLCT ($L_\sigma \rightarrow L_{\sigma*}$). The second-largest contribution comes from orbital pair (51*a*, 54*a*), where 51*a* is the HOMO−3 [0.47p(L) + 0.23p(S) + 0.15d(Re)] and 54*a* is the LUMO+2 [0.55d(Re) + 0.23p(O) + 0.18p(S)]. The orbital components of L fragments [p(L)], which are involved mainly in the occupied 51*a* (47%) is absent in the virtual orbital 54*a*, indicating its electron-donor character. The relevant electronic transition processes are again LMCT (dominant), MMCT, and LLCT, similar to those of the (51*b*, 52*b*) transition. The third-largest contribution comes from the (50*a*, 54*a*) transition. Different from the 51*a* orbital, 50*a* locates mostly on L fragments and dirhenium without the components of p(O) and p(S). The relevant transition processes can be assigned to LMCT, MMCT, and LLCT as well. L fragments clearly play the role of the electronic donor in the LMCT and LLCT, and S and O atoms clearly play the electronic acceptor in LLCT. The above three orbital-pair transitions make positive contributions to the magnitude of the β values. They give priority to LMCT processes, but MMCT and metal-inductive LLCT processes are impressive. They are all involved in the lower-energy excitations (in the range from 2.1 to 3.6 eV). However, the contribution of the orbital-pair transition (49*b*, 53*b*) is the second-largest in magnitude with a relative ratio of 74%, but it is negative; that is, it would reduce rather than enhance the given component of the quadratic hyperpolarizability. This orbital-pair transition is involved in the higher-energy excitations (in the range from 3.6 to 3.8 eV). The orbital 49*b* has large components of p(O) and p(S). The d orbital components of dirhenium are only about 10% in total. In the virtual orbital 53*b*, however, the d-orbital components of dirhenium enhance to 55% in total, whereas the p(O) components decrease greatly. The relevant electronic transition processes are thus assigned to LMCT ($L_\sigma \rightarrow d_{\sigma*}$), MMCT (($d_\delta \rightarrow d_{\delta*}$) and LLCT [p(O) → p(S)]. It is worth noting that the contributions of the L fragments are absent. The other negative contributor is orbital pair (49*b*, 54*b*). Its contribution in magnitude has a relative ratio of about 18% to the largest one. The analysis shows a situation similar to that of orbital pair (49*b*, 53*b*) and will not be described in detail for clarity. It also involves the LMCT, MMCT, and LLCT processes missing the contribution of L fragments.

In a word, the main CT process contributing to the quadratic hyperpolarizability of model **2** is the LMCT process, which is completely different from the situation in model **1**. If L fragments participate in the LMCT process as the electron donors in addition to the oxo and sulfide ligands, then the contribution would be positive or vice versa. The MMCT has been confirmed to be one of the transition processes that plays roles in the enhancement of the β values.

4. Conclusions

In this article, the electronic structures and response properties of two typical dirhenium metal cluster complexes have been investigated intensively based on the high-level DFT/TDDFT calculations and the orbital-decomposition scheme. The direct metal-to-metal transition process has been unambiguously confirmed to be one of the NLO response mechanisms of these two dinuclear complexes.

We summarized some important results as follows: (*i*) Multiple electronic transition processes exist that collectively contribute to the quadratic hyperpolarizability of these two dirhenium clusters including MLCT/LMCT, MMCT, and metal-inductive LLCT. They have already been confirmed and described in the studies of organometallic and mononuclear NLO-phores[42] *except* MMCT, which is featured in the NLO response mechanism of these dinuclear clusters. The multiple transition processes are either cooperative to each other, such as the MLCT and MMCT synergetically enhancing the β value of model **1**, or are destructively interfering with each other, such as LMCT and MMCT making opposite contributions to the β value of model **2**. Our result indicates that the traditional two-level model no longer seems valid for the complex polynuclear metal clusters because multiple excited states (not only one) are coupled to the ground state to contribute to the β. (*ii*) The ratio of the β value related to the MMCT excitations (noted as β_{MMCT}) with respect to the global β value (β_{CT}), that is, β_{MMCT}/β_{CT}, seems to be related to the strength of the Re−Re interaction. Model **1** consists of the stronger Re−Re bonding, and the ratio of β_{MMCT}/β_{CT} is much larger than that of model **2**, which contains a weaker Re−Re interaction. This can be understood in terms of the electronic structures of the two models with different metal−metal interactions. In model **1**, the frontier MOs are dominated by the splitting d−d levels of dirhenium. Alternatively, in model **2** where the Re−Re interaction is weak, the predominant character of the frontier MOs involves more p/sp components of the ligands. (*iii*) The smaller β value of model **1** compared to that of model **2** takes place with the retention of essentially identical structural constraints of these two dimerized clusters. The dimeric character of dirhenium restricts sufficient transitions between the two equivalent rhenium atoms and hence results in small β_{MMCT} values of both models. Because the ratio of β_{MMCT}/β_{CT} is significant in model **1** as described above, the β_{CT}(**1**) is small. In contrast to model **1**, the main β-related CT process in model **2** is LMCT, which is not restricted by the dimerized structural symmetry. Consequently, model **2** could possess a large β_{CT} value although the β_{MMCT} of model **2** is also small. (*iv*) The first optically intense excitations (λ_{max}) of both models involve d−d transitions. The $d_{\delta*} \rightarrow d_{\pi*}$ is assigned to the λ_{max} (461 nm) excitation of model **1**, which agreed with the experimental reports on the strongly bound dirhenium cluster complexes. The percent component of the d → d transition in the first intense excitation is reduced greatly in model **2** basically because of the weaker Re−Re interaction. The LMCT in this case takes the dominant position, which agrees with the relevant experimental report of Kaim et al.[43]

The revealed unprecedented NLO-response mechanism related to the direct metal−metal interactions implies that the coordination polynuclear metal cluster is a promising area for NLO material exploration. The excitation properties and the second-order NLO activities of polynuclear metal cluster compounds can be modulated effectively through structural design of the metal core building block and metal substituents. The size and degree of delocalized π-conjugated ligands and the strength of the molecular dipole moments are not any longer the critical inquiries for the large quadratic hyperpolarizability. This would be beneficial in searching the novel metal-based NLO-phores possessing the improved tradeoffs between quadratic hyperpolarizability and optical absorption as well as crystallinity. This study improves our understanding of the detailed relationship between the direct metal−metal interaction and second-order optical nonlinearity and opens a way to further investigation in polynuclear clusters for novel second-order NLO materials and optical molecular devices.

Acknowledgment. We acknowledge the financial support from MOST projects (2006DFA43020 and 2007CB815307) and NSFC project (20573114).

Supporting Information Available: The Cartesian coordinates of models **1** and **2**. The HOMO contour of model **1** viewed from the *y* axis. The frontier molecular orbital contours of both models viewed from the *z* axis. This Information is available free of charge via the Internet at http://pubs.acs.org.

References and Notes

(1) (a) di Bella, S. *Chem. Soc. Rev.* **2001**, *30*, 355–366. (b) Powell, C. E.; Humphery, M. G. *Coord. Chem. Rev.* **2004**, *248*, 725–756. (c) Cariati, E.; Pizzotti, M.; Roberto, D.; Tessore, F.; Ugo, R. *Coord. Chem. Rev.* **2006**, *250*, 1210–1233. (d) Coe, B. J. *Acc. Chem. Res.* **2006**, *39*, 383–393, and the references therein. (e) Morrall, J. P. L.; Humphrey, M. G.; Dalton, G. T.; Cifuentes, M. P.; Samoc, M. In *Nonlinear Optical Properties of Matter, From Molecules to Condensed Phases*; Padadopoulos, M. G., Sadlej, A. J., Leszczynski, J., Eds.; Springer: Dordrecht, The Netherlands, 2006; pp 537−570, and the references therein. (f) Coe, B. J. In *Nonlinear Optical Properties of Matter, From Molecules to Condensed Phases*; Padadopoulos, M. G., Sadlej, A. J., Leszczynski, J., Eds.; Springer: Dordrecht, The Netherlands, 2006; pp 571−608, and the references therein.

(2) (a) Long, N. J. *Angew. Chem., Int. Ed. Engl.* **1995**, *34*, 21. (b) Barlow, S.; Bunting, H. E.; Ringham, C.; Green, J. C.; Bublitz, G. U.; Boxer, S. G.; Perry, J. W.; Marder, S. R. *J. Am. Chem. Soc.* **1999**, *121*, 3715–3723. (c) Maya, E. M.; Garcia-Frutos, E. M.; Vazquez, P.; Torres, T.; Martin, G.; Rojo, G.; Agullo-Lopez, F.; Gonzalez-Jonte, R. H.; Ferro, V. R.; Garcia de la Vega, J. M.; Ledoux, I.; Zyss, J. *J. Phys. Chem. A* **2003**, *107*, 2110–2117. (d) Senechal-David, K.; Hemeryck, A.; Tancrez, N.; Toupet, L.; Williams, J. A. G.; Ledoux, I.; Zyss, J.; Boucekkine, A.; Guegan, J. P.; Bozec, H. L.; Maury, O. *J. Am. Chem. Soc.* **2006**, *128*, 12243–12255. (e) Gradinaru, J.; Forni, A.; Druta, V.; Tessore, F.; Zecchin, S.; Quici, S.; Garbalau, N. *Inorg. Chem.* **2007**, *46*, 884–895.

(3) (a) Liao, Y.; Eichinger, B. E.; Firestone, K. A.; Haller, M.; Luo, J.; Kaminsky, W.; Benedict, J. B.; Reid, P. J.; Jen, A. K.-Y.; Dalton, L. R.; Robinson, B. H. *J. Am. Chem. Soc.* **2005**, *127*, 2758–2766. (b) Tessore, F.; Roberto, D.; Ugo, R.; Mussini, P.; Quici, S.; Ledoux-Rak, I.; Zyss, J. *Angew. Chem., Int. Ed* **2003**, *42*, 456–459. (c) Coe, B. J.; Harris, J. A.; Brunschwig, B. S. *J. Phys. Chem.* **2002**, *106*, 897.

(4) Frasier, C. C.; Harvey, M. A.; Cokerham, M. P.; Hand, H. M.; Chauchard, E. A.; Lee, C. H. *J. Phys. Chem.* **1986**, *90*, 5703–5706.

(5) Green, M. L.; Marder, S. R.; Thompson, M. E.; Bandy, J. A.; Bloor, D.; Kolinsky, P. V.; Jones, R. J. *Nature* **1987**, *330*, 360–362.

(6) (a) LeCours, S. M.; Guan, L.-W.; DiMagno, S. G.; Wang, C. H.; Therien, M. J. *J. Am. Chem. Soc.* **1996**, *118*, 1497–1503. (b) Senge, M. O.; Fazekas, M.; Notaras, E. G. A.; Blau, W. J.; Zawadzka, M.; Locos, O. B.; Ni Mhuircheartaigh, E. M. *Adv. Mater.* **2007**, *19*, 2737–2774.

(7) Coe, B. J.; Harries, J. L.; Harris, J. A.; Brunschwig, B. S.; Horton, P. N.; Hursthouse, M. B. *Inorg. Chem.* **2006**, *45*, 11019–11029.

(8) Maury, O.; Viau, L.; Senechal, K.; Corre, B.; Guegan, J. P.; Renouard, T.; Ledoux, I.; Zyss, J.; Le Bozec, H. *Chem.−Eur. J.* **2004**, *10*, 4454.

(9) (a) Coe, B. J.; Jones, L. A.; Harris, J. A.; Brunschwig, B. S.; Asselberghs, I.; Clays, K.; Persoons, A.; Garin, J.; Orduna, J. *J. Am. Chem. Soc.* **2004**, *126*, 3880–3891. (b) Ray, P. C. *Chem. Phys. Lett.* **2004**, *394*, 354–360.

(10) Cotton, F. A.; Murillo, L. A.; Walton, R. A. *Multiple Bonds between Metal Atoms*; Springer Science: New York, 2005.

(11) Cotton, F. A.; Harris, C. B. *Inorg. Chem.* **1965**, *4*, 330–333.

(12) (a) Kreisel, K. A.; Yap, G. P. A.; Dmitrenko, O.; Landis, C. R.; Theopold, K. H. *J. Am. Chem. Soc.* **2007**, *129*, 14162–14163. (b) Nguyen, T.; Sutton, A. D.; Brynda, M.; Fettinger, J. C.; Long, G. J.; Power, P. P. *Science* **2005**, *310*, 844–847.

(13) (a) Roos, N. O.; Antonio, C.; Borin, A. C.; Gagliardi, L. *Angew. Chem., Int. Ed.* **2007**, *46*, 1469–1472. (b) Frenking, G.; Tonner, R. *Nature* **2007**, *446*, 276–277.

(14) (a) Yam, V. W. *Acc. Chem. Res.* **2002**, *35*, 555–563. (b) Watson, D. F.; Tan, H. S.; Schreiber, E.; Mordas, C. J.; Bocarsly, A. B. *J. Phys. Chem. A* **2004**, *108*, 3261–3267. (c) Bernhardt, P. V.; Bozoglian, F.; Macpherson, B. P.; Martinez, M. *Coord. Chem. Rev.* **2005**, *249*, 1902–1916. (d) Bernhardt, P. V.; Bozoglian, F.; Gonzalez, G.; Martinez, M.; Macpherson, B. P.; Sienra, B. *Inorg. Chem.* **2006**, *45*, 74–82. (e) Santi, S.; Orian, L.; Durante, C.; Bisello, A.; Benetollo, F.; Crociani, L.; Ganis, P.; Ceccon, A. *Chem.−Eur. J.* **2007**, *13*, 1955–1968. (f) Grirrane, A.; Resa, I.; Rodriguez, A.; Carmona, E.; Alvarez, E.; Gutierrez-Puebla, E.; Monge, A.; Galindo, A.; del Rio, D.; Andersen, R. A. *J. Am. Chem. Soc.* **2007**, *129*, 693–703.

(15) (a) Fornies, J.; Fuertes, S.; Martin, A.; Violeta Sicilia, V.; Lalinde, E.; Moreno, M. T. *Chem.−Eur. J.* **2006**, *12*, 8253–8266. (b) Petitjean, A.; Puntoriero, F.; Campagna, S.; Juris, A.; Lehn, J. M. *Eur. J. Inorg. Chem.* **2006**, 3878–3892. (c) Lin, W.; Frei, H. *J. Am. Chem. Soc.* **2005**, *127*, 1610–1611. (d) Nakamura, R.; Okamoto, A.; Osawa, H.; Irie, H.; Hashimoto, K. *J. Am. Chem. Soc.* **2007**, *129*, 9596–9597.

(16) (a) Laidlaw, W. M.; Denning, R. G.; Verbiest, T.; Chauchard, E.; Persoons, P. *Nature* **1993**, *363*, 58. (b) Laidlaw, W. M.; Denning, R. G.; Verbiest, T.; Chauchard, E.; Persoons, P. *Proc. SPIE-Int. Soc. Opt. Eng.* **1994**, *2143*, 14.

(17) For example, Jayaprakash, K. N.; Ray, P. C.; Matsuoka, I.; Bhadbhade, M. M.; Puranik, V. G.; Das, P. K.; Nishihara, H.; Sarkar, A. *Organometallics* **1999**, *18*, 3851–3858.

(18) (a) Meyer-Friedrichsen, T.; Wong, H.; Prosenc, M. H.; Heck, J. *Eur. J. Inorg. Chem.* **2003**, 936–946. (b) Mang, C. Y.; Huang, B. S.; Liu, C. P.; Wu, K. C. *J. Mol. Struct.: THEOCHEM* **2007**, *808*, 145–152.

(19) (a) Shi, S.; Ji, W.; Tang, S. H.; Lang, J. P.; Xin, X. Q. *J. Am. Chem. Soc.* **1994**, *116*, 3615–3616. (b) Shi, S.; Ji, W.; Lang, J. P.; Xin, X. Q. *J. Phys. Chem.* **1994**, *98*, 3570–3572. (c) Shi, S.; Chen, H.; Hou, H.; Xin, X. Q.; Yu, K. *Chem. Mater.* **1995**, *7*, 1519–1524.

(20) (a) Wu, J.; Zhang, C.; Song, Y. L.; Zhang, E. P.; Hou, H. W.; Fan, Y.; Zhu, Y. *Chem.−Eur. J.* **2006**, *12*, 5823–5831. (b) Liang, K.; Zheng, H. G.; Song, Y. L.; Li, Y. Z.; Xin, X. Q. *Cryst. Growth Des.* **2007**, *7*, 373–376.

(21) Zhang, C.; Song, Y. L.; Wang, X. *Coord. Chem. Rev.* **2007**, *251*, 111–141.

(22) (a) Chen, X. H.; Wu, K. C.; Snijders, J. G.; Lin, C. S. *Inorg. Chem.* **2003**, *42*, 532–540. (b) Wu, K. C.; Sa, R. J.; Lin, C. S. *New J. Chem.* **2005**, *29*, 362–365.

(23) Zhou, Z. F.; Zhuang, B. T.; Wu, K. C.; Liu, P.; Wei, Y. Q. *J. Organomet. Chem.* **2007**, *692*, 1411–1420.

(24) (a) Dequeant, M. Q.; Bradley, P. M.; Xu, G. L.; Lutterman, D. A.; Turro, C.; Ren, T. *Inorg. Chem.* **2004**, *43*, 7887–7892. (b) Barclay, T.; Eglin, J. L.; Smith, L. T. *Polyhedron* **2001**, *20*, 767–771. (c) Golichenko, A. A.; Shtemenko, A. V. *Russ. J. Coord. Chem.* **2006**, *32*, 242–249.

(25) Masters, A. F.; Mertis, K.; Gibson, J. F.; Wilkinson, G. *Nouveau J. Chim.* **1977**, *1*, 389.

(26) Cotton, F. A.; Extine, M. W. *J. Am. Chem. Soc.* **1978**, *100*, 3788–3792.

(27) Cai, S.; Hoffman, D. M.; Wierda, D. A. *Inorg. Chem.* **1991**, *30*, 827–831.

(28) Hieringer, W.; Baerends, E. J. *J. Phys. Chem. A* **2006**, *110*, 1014–1021.

(29) Li, Q. H.; Sa, R. J.; Liu, C. P.; Wu, K. C. *J. Phys. Chem. A* **2007**, *111*, 7925–7932.

(30) (a) Becke, A. D. *Phys. Rev. A* **1988**, *38*, 3098. (b) Perdew, J. P. *Phys. Rev. B* **1988**, *33*, 8822.

(31) (a) Ceperly, D. M.; Alder, B. J. *Phys. Rev. Lett.* **1980**, *45*, 566. (b) Vosko, S. H.; Wilk, L.; Nusair, M. *Can. J. Phys.* **1980**, *58*, 1200.

(32) Stoll, H.; Pavlidou, C. M. E.; Preuss, H. *Theor. Chim. Acta* **1978**, *49*, 143.

(33) (a) van Lenthe, E.; Baerends, E. J.; Snijders, J. G. *J. Chem. Phys.* **1993**, *99*, 4597. (b) van Lenthe, E.; Baerends, E. J.; Snijders, J. G. *J. Chem. Phys.* **1996**, *105*, 6505. (c) van Lenthe, E.; Ehlers, A. E.; Baerends, E. J. *J. Chem. Phys.* **1999**, *110*, 8943.

(34) (a) van Gisbergen, S. J. A.; Snijders, J. G.; Baerends, E. J. *J. Chem. Phys.* **1998**, *109*, 10644–10656. (b) te Velde, G.; Bickelhaupt, F. M.; Baerends, E. J.; Fonseca-Guerra, C.; van Gisbergen, S. J. A.; Snijders, J. G.; Ziegler, T. *J. Comput. Chem.* **2001**, *22*, 931.

(35) (a) van Gisbergen, S. J. A.; Snijders, J. G.; Baerends, E. J. *J. Chem. Phys.* **1998**, *109*, 10644. (b) van Gisbergen, S. J. A.; Snijders, J. G.; Baerends, E. J. *Comput. Phys. Commun.* **1999**, *118*, 119.

(36) Gruning, M.; Gritsenko, O. V.; van Gisbergen, S. J. A.; Baerends, E. J. *J. Chem. Phys.* **2001**, *114*, 652.

(37) van Leeuwen, R.; Baerends, E. J. *Phys. Rev. A* **1994**, *49*, 2421.

(38) Karton, A.; Iron, M. A.; van der Boom, M. E.; Martin, J. M. L. *J. Phys. Chem. A* **2005**, *109*, 5454–5462.

(39) Inerbaev, T. M.; Belosludov, R. V.; Mizuseki, H.; Takahashi, M.; Kawazoe, Y. *J. Chem. Theory Comput.* **2006**, *2*, 1325–1334.

(40) Mayer, I. *Chem. Phys. Lett.* **1983**, *97*, 270–274.

(41) Landis, C. R.; Weinhold, F. *J. Am. Chem. Soc.* **2006**, *128*, 7335–7345.

(42) (a) Maury, O.; Le Bozec, H. *Acc. Chem. Res.* **2005**, *38*, 691–704. (b) Tessore, F.; Roberto, D.; Ugo, R.; Pizzotti, M.; Quici, S.; Cavazzini, M.; Bruni, S.; De Angelis, F. *Inorg. Chem.* **2005**, *44*, 8967–8978. (c) Senechal-David, K.; Hemeryck, A.; Tancrez, N.; Toupet, L.; Williams, J. A. G.; Ledoux, I.; Zyss, J.; Boucekkine, A.; Guegan, J. P.; Bozec, H. L.; Maury, O. *J. Am. Chem. Soc.* **2006**, *128*, 12243–12255.

(43) Schafer, R.; Kaim, W.; Fiedler, J. *Inorg. Chem.* **1993**, *32*, 3199–3200.

JP712156T